


Prediction of Pharmacokinetic Drug–Drug Interactions Involving Anlotinib as a Victim by Using Physiologically Based Pharmacokinetic Modeling

Fengjiao Bu^{1,2,*}, Yong-Soon Cho^{3,4,*}, Qingfeng He¹, Xiaowen Wang¹, Saurav Howlader^{3,4}, Dong-Hyun Kim^{3,4}, Mingshe Zhu⁵, Jae Gook Shin^{3,4}, Xiaoqiang Xiang^{1,6} 

¹Department of Clinical Pharmacy and Pharmacy Administration, School of Pharmacy, Fudan University, Shanghai, People's Republic of China;

²Department of Pharmacy, Eye and ENT Hospital, Fudan University, Shanghai, People's Republic of China; ³Department of Pharmacology and Pharmacogenomics Research Center, Inje University College of Medicine, Busan, Republic of Korea; ⁴Center for Personalized Precision Medicine of Tuberculosis, Inje University College of Medicine, Busan, Republic of Korea; ⁵Department of DMPK, MassDefect Technologies, Princeton, NJ, USA;

⁶Department of Preclinical Evaluation, Quzhou Fudan Institute, Quzhou, Zhejiang Province, 324002, People's Republic of China

*These authors contributed equally to this work

Correspondence: Jae Gook Shin; Xiaoqiang Xiang, Email phshinj@gmail.com; xiangxq@fudan.edu.cn

Background: Anlotinib was approved as a third line therapy for advanced non-small cell lung cancer in China. However, the impact of concurrent administration of various clinical drugs on the drug–drug interaction (DDI) potential of anlotinib remains undetermined. As such, this study aims to evaluate the DDI of anlotinib as a victim by establishing a physiologically based pharmacokinetic (PBPK) model.

Methods: The PBPK model of anlotinib as a victim drug was constructed and validated in the Simcyp[®] incorporating parameters derived from in vitro studies, pre-clinical investigations, and clinical research encompassing patients with cancer. Subsequently, plasma exposure of anlotinib in cancer patients was predicted for single- and multi-dose co-administration with typical perpetrators mentioned in Food and Drug Administration (FDA) industrial guidance.

Results: Based on predictions, the CYP3A potent inhibitor ketoconazole demonstrated the most significant DDI with anlotinib, regardless of whether anlotinib is administered as a single dose or multiple doses. Ketoconazole increased the area under the concentration-time curve (AUC) and maximum concentration (C_{max}) of single-dose anlotinib to 1.41-fold and 1.08-fold, respectively. In contrast, rifampicin, a potent inducer of CYP3A enzymes, exhibited a relatively higher level of DDI, with AUC_R and C_{maxR} values of 0.44 and 0.79, respectively.

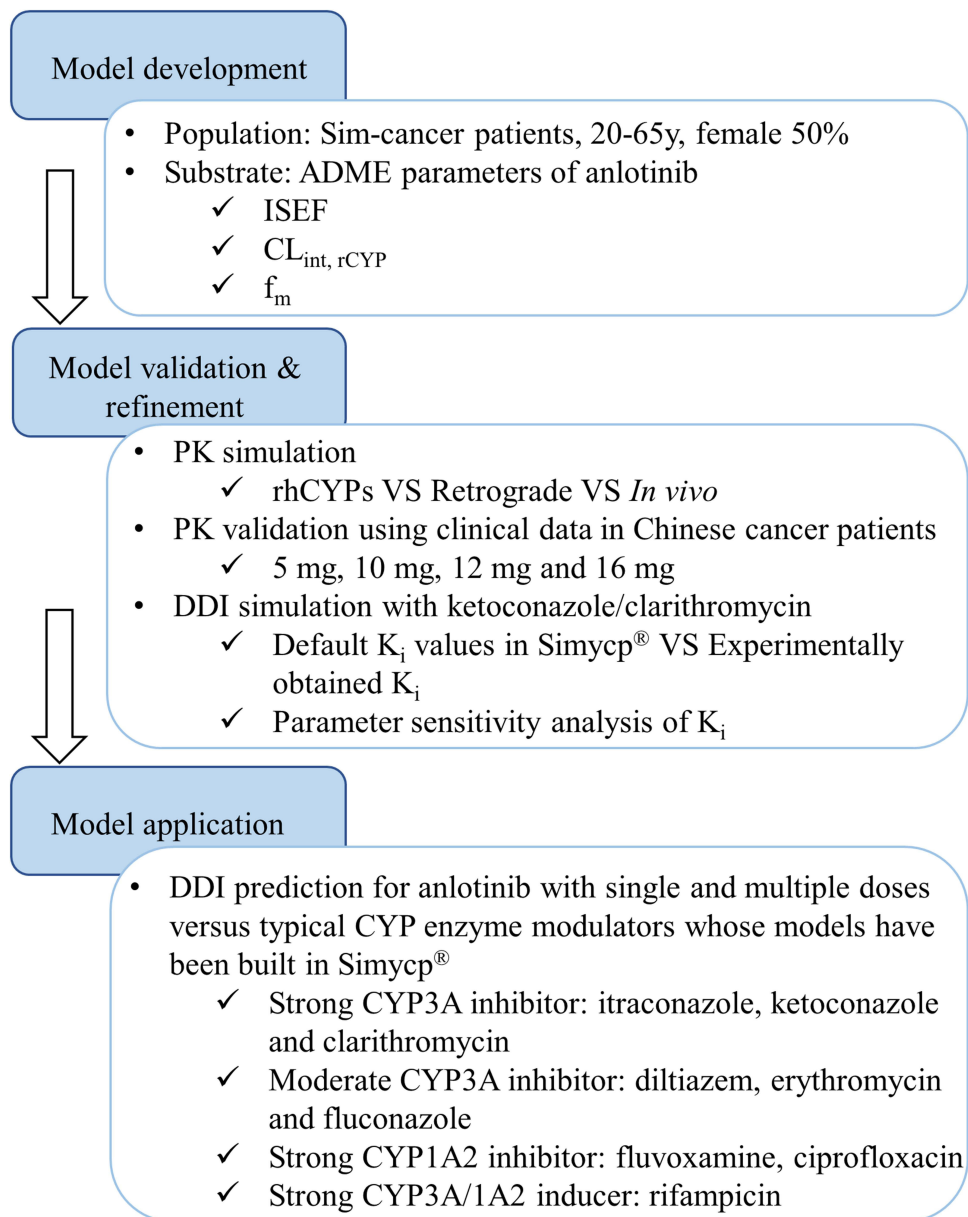
Conclusion: Based on the PBPK modeling, there is a low risk of DDI between anlotinib and potent CYP3A/1A2 inhibitors, but caution and enhanced monitoring for adverse reactions are advised. To mitigate the risk of anti-tumor treatment failure, it is recommended to avoid concurrent use of strong CYP3A inducers. In conclusion, our study enhances understanding of anlotinib's interaction with medications, aiding scientists, prescribers, and drug labels in gauging the expected impact of CYP3A/1A2 modulators on anlotinib's pharmacokinetics.

Keywords: anlotinib, DDIs, CYP3A, CYP1A2, PBPK

Introduction

According to the American Cancer Society's cancer statistics estimates, lung cancer remains the leading cause of cancer-related deaths in 2022, with 80–85% of cases being non-small cell lung cancer (NSCLC).^{1,2} Conventional platinum-based chemotherapy regimens for NSCLC have limited efficacy, with a less than 5% 5-year survival rate.³ Targeted therapies, particularly tyrosine kinase inhibitors (TKIs), provide new avenues for the management of NSCLC. Over the

Graphical Abstract



past decade, nearly 20 new TKIs have been approved by regulatory bodies, such as the European Medicines Agency and Food and Drug Administration (FDA).¹

Anlotinib, a recently developed small molecule multi-target TKI, has demonstrated efficacy in suppressing the activity of various receptors including vascular endothelial growth factor receptor, platelet-derived growth factor receptor, fibroblast growth factor receptor and c-Kit. The National Medical Products Administration (NMPA) granted its approval for the treatment of NSCLC in third-line therapy in 2018. Previous studies and drug package inserts have demonstrated that anlotinib exhibits non-substrate characteristics towards P-gp and is primarily metabolized by CYP1A2 and CYP3A4/5, with minor contributions from CYP2B6, CYP2C8, CYP2C9, CYP2C19, and CYP2D6.⁴ The drug label cautions against concomitant administration with inhibitors and inducers of CYP1A2 and CYP3A4/5.⁵ In our previous study, a PBPK model of anlotinib was established to elucidate its interaction potential as a perpetrator. The simulations

showed a very low likelihood of anlotinib inducing clinically significant DDIs.⁶ It is noteworthy that no formal drug interaction assessments have been undertaken for anlotinib. Thus, the impact of CYP inducers and inhibitors on anlotinib's plasma exposure is unclear.

The PBPK model represents a mathematical modeling strategy that employs inputs derived from anatomical structure, physiology, and biochemical parameters to forecast drug pharmacokinetics *in silico*.⁷ PBPK modeling and simulation have been extensively utilized over the last two decades in every stage of drug development, including the selection of early compounds for first-in-human trials and evaluation of DDIs for labeling purposes. From 2008 to 2017, the FDA received 130 investigational new drug applications and 94 new drug applications that included PBPK analyses.⁸ Moreover, PBPK modeling was also recommended in the FDA guidelines for clinical DDI studies.⁹

This study aims to assess the drug interactions involving anlotinib as a victim to provide guidance for clinical co-administration. To achieve this objective, we first utilized *in vitro* half-life assays to determine the intrinsic clearance of anlotinib in human liver microsomes (HLM) and human recombinant CYP isoforms (rhCYPs). Moreover, the contribution of specific CYP enzymes to the total human liver microsomal intrinsic clearance was assessed. Subsequently, we integrated the relevant parameters into the established PBPK model, which was then employed to predict the impact of CYP enzyme modulators on the plasma exposure of anlotinib in patients with cancer.

Materials and Methods

Materials

Anlotinib was purchased from Selleckchem (Houston, TX, USA) under the lot number S872601, while 1-OH-midazolam (1-JLI-64-2) and clarithromycin (Lot No. 26-SSR-179-1) were obtained from Toronto Research Chemicals (North York, Canada). Phenacetin (Lot No. LRAA9053), acetaminophen (Lot No. MKCD6375), midazolam (Lot No. BCCH1232), ketoconazole (Cat No. LRAA9173), and levofloxacin (lot number 038M4848V) were purchased from Sigma-Aldrich (St. Louis, MO). β -NADP (β -nicotinamide adenine dinucleotide phosphate), EDTA, $MgCl_2$, G6P (glucose 6-phosphate), G6PD (glucose-6-phosphate dehydrogenase) were purchased from Sigma-Aldrich (St. Louis, MO). Acetonitrile was obtained from Fisher Scientific (Pittsburgh, PA). All the reagents and chemicals were of the highest quality available. Pooled HLMs (Lot No. 1151001) and the baculovirus-insect cell-expressed human CYPs 1A2 (Lot No. 20062301), 2B6 (Lot No. 19111503), 2C8 (Lot No. 20062302), 2C9 (Lot No. 19071101), 2C19 (Lot No. 19072601), 2D6 (Lot No. 20051301), 3A4 (Lot No. 20062303), and 3A5 (Lot No. 19041703) were obtained from SPMED CO., Ltd (Busan, Republic of Korea) and Corning (NY, USA), with information about protein concentration and P450 isoform content provided by the manufacturer.

In vitro Metabolic Stability Assays of Anlotinib by HLM and rhCYPs

Stock solutions of anlotinib, clarithromycin, and ketoconazole were prepared in dimethyl sulfoxide (DMSO). Stock solutions of acetaminophen, levofloxacin, and midazolam were prepared in methanol. All stock solutions were stored at $-20^{\circ}C$ prior to use. For metabolic stability of anlotinib, incubation mixtures containing 1 μM anlotinib, 0.5 mg HLM protein/mL or rhCYPs (20 pmol/mL), and 0.1 M potassium phosphate buffer (pH 7.4) were mixed and preincubated for 5 min at $37^{\circ}C$. To initiate the reaction, an NADPH-generating system that was comprising 3.3 mM G6P, 1.3 mM β -NADP⁺, 3.3 mM $MgCl_2$, and 1.0 unit/mL glucose-6 phosphate dehydrogenase (G6PDH) was added, and the incubation mixtures (final volume 1000 μL) were incubated for 60 min at $37^{\circ}C$ in a shaking water bath. The aliquots (100 μL) were taken at different time points and the reaction was terminated by adding 100 μL of acetonitrile containing imatinib as an internal standard. The incubation mixtures were centrifuged at 13,200g for 5 min at $4^{\circ}C$. Each incubation was performed in triplicate. Aliquots (5 μL) of the supernatants were analyzed by high-performance liquid chromatography-tandem mass (HPLC-MS/MS). Linear regression was performed by the residual percentage of anlotinib against incubation time. Then, the intrinsic clearance (CL_{int}) was calculated according to the Equations 1 and 2.^{10,11}

$$In\ vitrot_{1/2} = \frac{\ln 2}{Slope} \quad (1)$$

$$CL_{int} = \frac{0.693}{\ln \text{ in vitro } t_{1/2}} \times \frac{1}{C_{\text{protein}}} \times 1000 (L/\text{min}/\text{mg protein or } L/\text{min}/\text{pmol}) \quad (2)$$

Determination of ISEF for rhCYP and f_m for the Major Metabolic Enzymes of Anlotinib

For scaling of recombinant CYP in vitro kinetic data, intersystem extrapolation factors (ISEF) for CYP1A2, CYP3A4, and CYP3A5 were measured using phenacetin, and midazolam as the probe substrate. The incubation mixture consisted of 20 pmol recombinant CYP1A2, CYP3A4/5, 25 μM phenacetin, midazolam and an NADPH generating system (1.3 mm β -nicotinamide adenine dinucleotide phosphate, 3.3 mm glucose 6-phosphate, 3.3 mm MgCl_2 and 1.0 unit/mL G6PDH) in a total volume of 100 μL phosphate buffer (0.1 M, pH 7.4). The reaction was initiated by the addition of the NADPH-generating system (20 μL) and continued in a water bath at 37°C for 15 min. Each reaction was performed in triplicate. The reaction was terminated by the addition of the same volume of acetonitrile. After centrifugation at 16,000g for 5 min, a 5 μL aliquot of the supernatant was injected directly into the HPLC-MS/MS system. Then, the ISEF values were calculated according to Equation 3.¹² $CL_{int, HLM}$ is the intrinsic clearance of a specific probe substrate by HLM; $CL_{int, rhCYP}$ is the intrinsic clearance of a typical probe substrate metabolized by a single CYP450 enzyme isoform; $HLM_{CYP \text{ abundance}}$ is the amount of a single CYP450 enzyme isoform in liver microsomes.

$$ISEF(CL_{int}) = \frac{CL_{int, HLM} (\mu L/\text{min}/\text{mg protein})}{CL_{int, rhCYP} (\mu L/\text{min}/\text{pmol CYP}) \times HLM_{CYP \text{ abundance}} (\text{pmol CYP}/\text{mg protein})} \quad (3)$$

Afterward, ISEF was used to assess the contribution of a specific CYP enzyme to the total human liver microsome (f_m). The relative contribution of individual rhCYP was calculated by Equation 4.¹³ CL_{int, CYP_i} is the intrinsic clearance of anlotinib metabolized by a specific recombinant P450 isoform. $\sum_i^n ISEF \times CL_{int, CYP_i}$ is the total intrinsic clearance of anlotinib by relevant recombinant P450 isoforms.

$$f_m(CYP_i) = \frac{ISEF \times CL_{int, CYP_i}}{\sum_i^n ISEF \times CL_{int, CYP_i}} \quad (4)$$

Determination of Reversible Inhibition Constant (K_i) of CYP3A/CYP1A2 on Anlotinib as a Substrate

Incubation mixture (final volume 100 μL) contained 0.1 M potassium phosphate buffer (pH 7.4), various concentrations of inhibitors (ketoconazole, clarithromycin or levofloxacin at 0, 0.5, 1, 5, 10, and 20 μM) and anlotinib (0.5, 1, 2, 5, and 10 μM) were pre-incubated with HLM (0.5 mg/mL), or rhCYPs (CYP3A4/5, CYP1A2 at 20 pmol/mL) for 5 min at 37°C in a shaking water bath. Then, reactions were initiated with the addition of an NADPH-generating system that was comprised of 3.3 mm G6P, 1.3 mm β -NADP+, 3.3 mm MgCl_2 and 1.0 unit/mL G6PDH. After a 60-min incubation, the reactions were terminated by the addition of 0.1 mL ice-cold acetonitrile followed by centrifugation at 13,200g for 10 min. Afterwards, 5 μL of the supernatant was analyzed by HPLC-MS/MS. Each incubation was performed in triplicate. Then Lineweaver-Burk plots were employed to determine the inhibition mechanism. A linear regression analysis of the slope against the inhibitor concentration was also performed to finally calculate the K_i values.

HPLC-MS/MS Analysis

A tandem quadrupole mass spectrometer (Agilent 6410 hPLC-MS/MS, Agilent, Santa Clara, CA) coupled with an Agilent 1200 series HPLC system was used to analyze the samples. The separation was performed with a XBridge BEH C18 column (2.1 mm \times 50 mm, 3.5 μm ; Milford, MA, USA), and a Luna C18 column (2 \times 50 mm, 3 μm ; Phenomenex, Torrance, California, USA). The aqueous mobile phase consisted of 0.1% formic acid in water (solvent A), and the organic mobile phase consisted of 0.1% formic acid in acetonitrile (solvent B). A gradient program was used for HPLC separation, with a flow rate of 0.2 mL/min. The total run time was 6.0 min. The initial composition of solvent B was 5%, which was increased to 80% after 2.0 min and maintained for 1.0 min, followed by re-equilibration to the initial

conditions for 3.0 min. Mass spectra were recorded by electrospray ionization with a positive mode. The turbo ion spray interface was operated at 4000 V and 300°C. The operating conditions were optimized by flow injection of an analyte and were determined as follows: nebulizing gas flow, 20 liters/min; curtain gas flow, 10 liters/min; and collision energy, 18 eV. Multiple-reaction monitoring (MRM) mode using a specific precursor/product ion transition was employed for the quantification. The detection of anlotinib, imatinib, acetaminophen, 1-OH-midazolam was performed by monitoring the transitions of m/z 408.2–339.1, 494.3–394.2, 152.0–120.0, 342.0–203.0, respectively. The peak areas for all compounds were automatically integrated using MassHunter quantitative analysis (version B.1.4).

Refinement and Validation of the PBPK Model of Anlotinib as a Victim

The PBPK model of anlotinib as a victim was developed by Simcyp® (version 18.1.0, Certara Ltd., Sheffield, United Kingdom). Sim-cancer populations were used for model development, the population size was 100 (10 trials × 10 subjects), and the proportion of females was 0.5, with an age range between 20 and 65 years old. The physicochemical parameters, absorption and distribution data of anlotinib remained the same as the recent article published by our research group, which has successfully predicted the pharmacokinetic interactions caused by anlotinib⁶, [Table S1](#) presents the detailed modeling parameters. In contrast to the PBPK model of anlotinib as a perpetrator, in the PBPK model of anlotinib as a victim, enzyme kinetic parameters of CYP1A2, CYP3A4 and CYP3A5 were added to simulate the pathways via which anlotinib was metabolized. In addition, a built-in retrograde tool of Simcyp® was utilized to back-calculate intrinsic clearance from in vivo CL_{po} and f_m for each rhCYP isoform. The CL_{po} in Chinese cancer volunteers was reported to be 11.014 L/h¹⁴. The percentages of anlotinib metabolized by CYP1A2, CYP3A4 and CYP3A5 were set at 35%, 35% and 29% respectively. Ultimately, the intrinsic hepatic clearance was calculated to be 0.44, 0.14 and 0.14 $\mu\text{L}/\text{min}/\text{pmol}$ for CYP1A2, CYP3A4 and CYP3A5 in the retrograde approach. Ultimately, ISEF-corrected $CL_{int, rhCYP}$ (obtained in-house) and retrograde $CL_{int, rhCYP}$ (retrograde calculator for back-calculating intrinsic clearance from in vivo CL or CL_{po}) were adopted to refine the PBPK model of anlotinib. To assess the accuracy of the PBPK model for anlotinib, both single-dose (5mg, 10mg, 12mg, and 16mg) and multiple-dose (12mg) administration regimens were employed. The validation of the established anlotinib model was based on clinical data obtained from published studies involving Chinese cancer patients.¹⁴ The dosing regimens adopted in PBPK model were consistent with published clinical trials. There were two treatment courses in multiple-dose administration regimen. And one treatment course was consisted of anlotinib 12mg once daily for 2 weeks followed by 1 week of discontinuation. The simulation was performed in a fasted state, as recommended by the anlotinib drug label, which suggests administration before breakfast. The accuracy of the PBPK model was verified by comparing the PK parameters predicted by the in vivo, rhCYP, and retrograde methods with the observed values reported in the literature.¹⁴ The fold error between the predicted value and the observed value was calculated according to Equation 5.¹⁵ Evaluation criteria are folded error within 0.5–2.

$$\text{Fold error} = \frac{\text{predicted value}}{\text{observed value}} \quad (5)$$

Application of the PBPK Model to Predict Anlotinib Pharmacokinetic Changes Caused by CYP Enzyme Modulators

The validated PBPK model was used to evaluate the potential risk of DDIs involving the CYP3A4/5 and CYP1A2-mediated metabolic pathways. For DDI prediction, kinetics parameters of rhCYP obtained in house were selected. Various perpetrators were then incorporated into the DDI model, encompassing potent inhibitors of CYP3A (itraconazole, ketoconazole, clarithromycin), moderate inhibitors of CYP3A (diltiazem, erythromycin, fluconazole), strong CYP1A2 inhibitors (fluvoxamine, ciprofloxacin), strong CYP3A and moderate CYP1A2 inducer (rifampicin). They are typical perpetrators mentioned in FDA industrial guidance, and their PBPK models were already constructed in Simcyp®. DDI parameters of perpetrators included in the PBPK-DDI model were listed in [Table S2](#). For the model application, simulations were conducted with “sim-cancer” population built into the software. The virtual population consisted of 100 individuals (10 trials × 10 subjects), evenly split between males and females, aged between 20 and 65 years. In the DDI prediction, both single and multiple doses of anlotinib were co-administered with various perpetrators. A single dose of anlotinib 12 mg was administered on Day 5 with an inhibitor or on Day 8 with an inducer. Administration strategies of typical CYP enzyme modulators were listed in the following [Table 1](#).

Table 1 The Administration Strategies of Typical CYP Enzyme Modulators

Category	Perpetrator	Dose (mg)	Dose Regimen
Strong CYP3A inhibitor	Itraconazole	200	q.d.
	Ketoconazole	400	q.d.
	Clarithromycin	250	b.i.d.
Moderate CYP3A inhibitor	Diltiazem	60	q.8.h.
	Fluconazole	200	q.d.
	Erythromycin	500	q.6.h.
Strong CYP1A2 inhibitor	Fluvoxamine	50	q.d.
	Ciprofloxacin	500	b.i.d.
Strong CYP3A/1A2 inducer	Rifampicin	600	q.d.

Co-administration regimens employed for predicting DDI between anlotinib and perpetrators were shown in [Figure S1](#). Both default K_i values in Simcyp[®] and K_i values obtained from experiment were used to simulate the interactions between anlotinib and ketoconazole (clarithromycin). To evaluate whether the DDI was significant, the criteria of AUC_R less than 0.5 (for induction) and greater than 2 (for inhibition) were adopted in this study.^{16,17} Moreover, a sensitivity analysis was also performed by adjusting K_i of ketoconazole from 0.015 to 11 (20 steps) for CYP3A4, and 0.109 to 11 (20 steps) for CYP3A5 to investigate the impact of K_i on the AUC ratio, as well as ciprofloxacin K_i adjusted from 0.2 to 20 (20 steps).

Results

CL_{int} of Anlotinib by HLM and rhCYPs

The metabolic stability of anlotinib in HLM and rhCYPs was shown in [Figure S2](#). The CL_{int} of anlotinib mediated by HLM is determined to be 18 $\mu\text{L}/\text{min}/\text{mg}$, indicating a moderate metabolic rate in humans. The depletion of anlotinib over incubation time was found not to be influenced by CYP2B6, 2C8, 2C9, 2C19, and 2D6. Instead, CYP1A2, 3A4 and 3A5 were the major CYP isozymes mediating the metabolism of anlotinib, with the CL_{int} of 0.23, 0.32, 0.31 $\mu\text{L}/\text{min}/\text{pmol}$ ([Figure 1](#)).

ISEF of rhCYPs and F_m of Anlotinib Metabolized by a Specific CYP Isoform

As listed in [Table 2](#), ISEF in our rhCYPs reaction system was 0.69 for CYP1A2, 0.49 for CYP3A4 and 0.43 for CYP3A5. Further, the f_m calculated from ISEF and $CL_{int,rhCYP}$ showed that CYP1A2 and CYP3A4 had the largest share of anlotinib metabolized by CYP450 with 35% for both. Followed by CYP3A5 with 29%. The contribution percentage of each rhCYP enzyme to whole CYP was depicted in a pie chart, as shown in [Figure 2](#).

K_i Values of the Inhibition of Anlotinib by Ketoconazole, Clarithromycin, and Levofloxacin

The inhibitory effects of ketoconazole, clarithromycin (CYP3A inhibitor), and levofloxacin (CYP1A2 inhibitor) on the activities of anlotinib at HLM and CYP isozymes were shown in [Figure 3](#). Each line of inhibitors intersected on the x-y side of the Lineweaver-Burk plots, indicating a mixed-type inhibition. It can be concluded that ketoconazole, clarithromycin, and levofloxacin are mixed inhibitors of anlotinib in HLMs with K_i values of 0.93 μM , 3.02 μM , 4.87 μM , respectively. The Lineweaver-Burk plots depicting the inhibition of CYP3A4 and CYP3A5 by ketoconazole revealed selective inhibition, with respective K_i values of 0.97 μM and 2.92 μM . Similarly, the Lineweaver-Burk plots representing the inhibition of CYP3A4 and CYP3A5 by clarithromycin exhibited K_i values of 3.52 μM and 6.88 μM , respectively. Moreover, the inhibition of CYP1A2 by levofloxacin was assessed, yielding a K_i value of 4.73 μM . The slope of the linear regression analysis against the inhibitor concentration is depicted in [Figure S3](#).

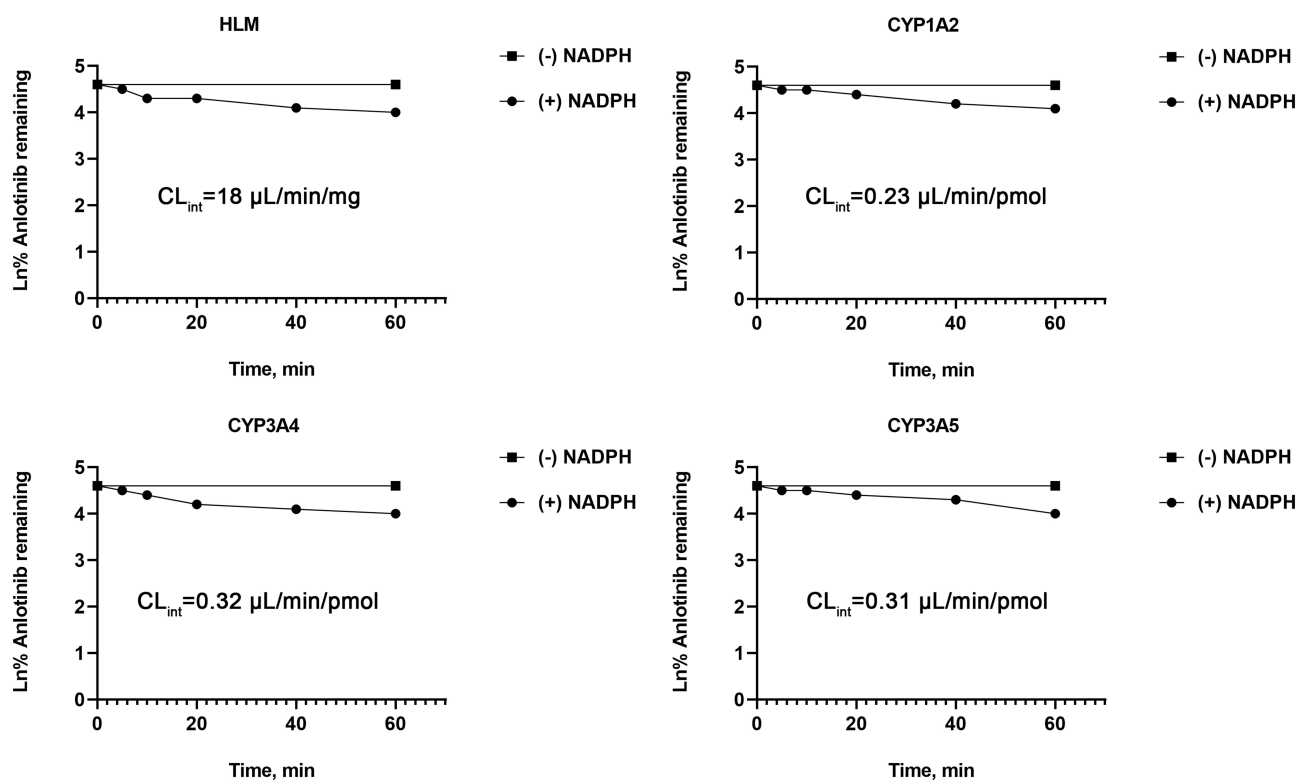


Figure 1 The residual percentage of anlotinib versus incubation time in HLM, CYP1A2, 3A4 and 3A5.

Simulation of Anlotinib as a Victim and DDI Simulations

Three approaches of *in vivo*, rhCYPs and retrograde models were used to simulate pharmacokinetic profiles of anlotinib in cancer patients. As seen in [Figure 4](#), both single dose and multiple doses of anlotinib at 12mg, the pharmacokinetic profile of the model simulation almost overlapped with that simulated using *in vivo* clearance data. The predictions for single doses of 5mg, 10mg and 16mg were also similar, seen in [Figure S4](#). Observed data are from pharmacokinetics in patients with advanced refractory solid tumors.¹⁴ Fold errors (ratio between predicted values from the rhCYP method and observed values) are almost consistently within a range of two-fold or less, shown in [Table S3](#).

The results of the DDI prediction in cancer patients were summarized in [Table 3](#). [Figures 5–8](#) displayed the DDIs resulting from the co-administration of strong CYP3A inhibitors, moderate CYP3A inhibitors, strong CYP1A2 inhibitors, and strong CYP3A/1A2 inducers, respectively. The simulation demonstrated that CYP inhibitors hardly caused significant change in the AUC and C_{max} of anlotinib regardless of single or multiple administration. Overall, the DDI effect of ketoconazole is most apparent among all CYP inhibitors. When anlotinib was administered as a single dose, the mean AUC and C_{max} ratios of anlotinib in cancer patients were found to be 1.41-fold and 1.08-fold, respectively.

Table 2 ISEF of CYP1A2, CYP3A4 and CYP3A5

rhCYP Isoform	Assay	CYP Content in rhCYP (pmolCYP/mg Protein)	Specific CYP Activity in HLM (Pmol/Min/Pmol)	ISEF
CYP1A2	Phenacetin O-deethylation	112.4	67.4	0.69
CYP3A4	Midazolam 1'-hydroxylation	113.63	12.4	0.49
CYP3A5	Midazolam 1'-hydroxylation	133.33	10.5	0.43

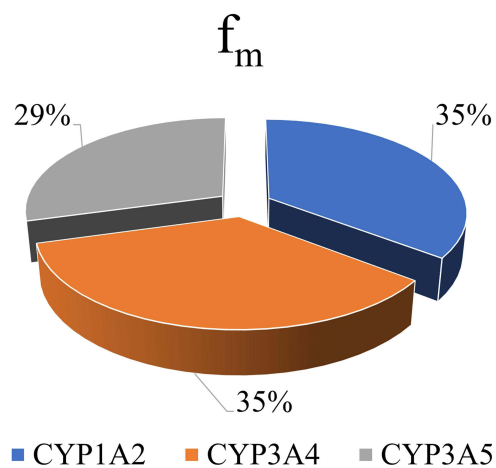


Figure 2 The f_m of in vitro CYP phenotyping.

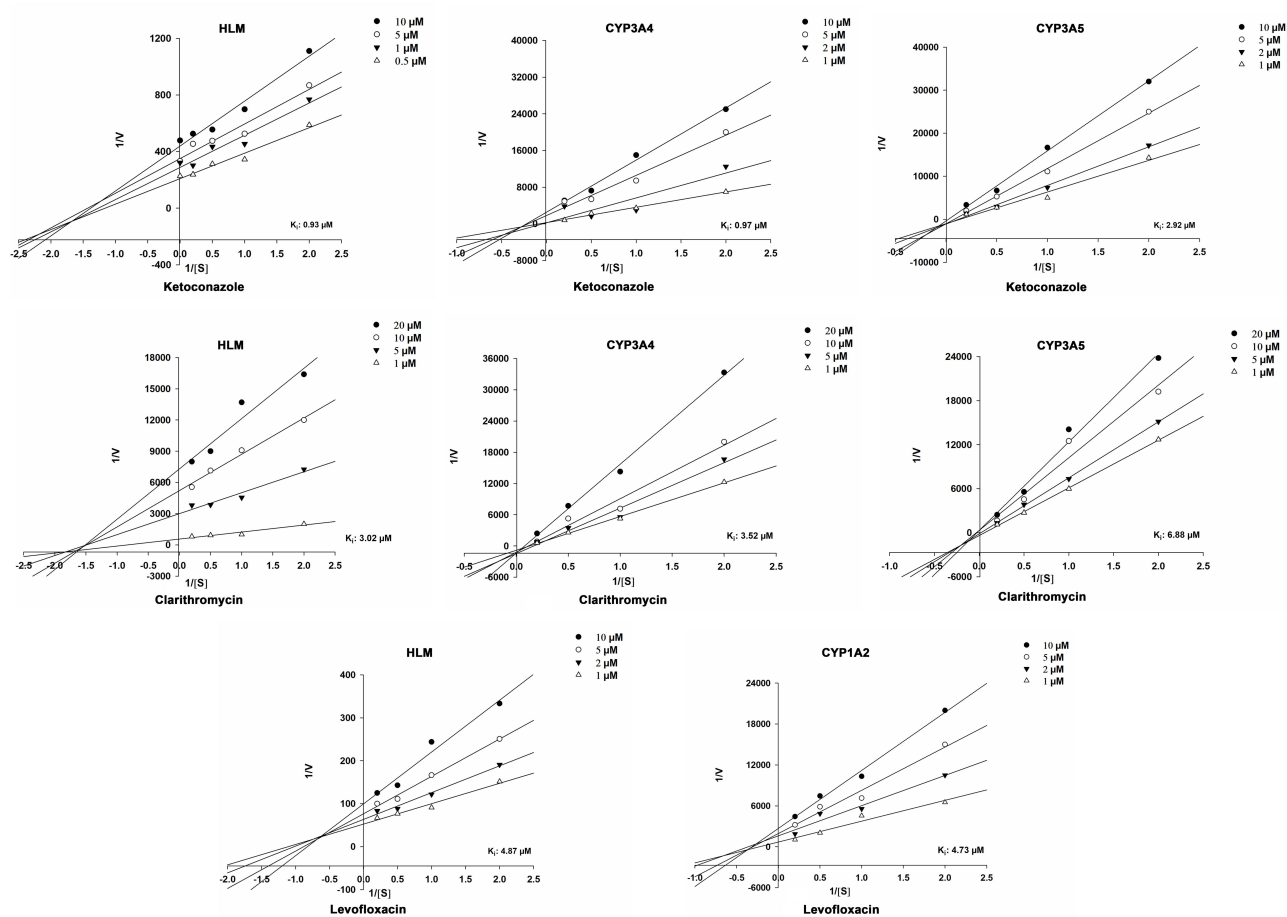


Figure 3 Lineweaver-Burk plots for the inhibition of HLM or rhCYPs by ketoconazole, clarithromycin, and levofloxacin. Various concentrations of anlotinib, ketoconazole, clarithromycin and levofloxacin were used. Each incubation was conducted in triplicate.

Comparable results were obtained when anlotinib was administered as multiple doses, with mean AUC and C_{max} ratios of 1.37-fold and 1.32-fold, respectively. In addition, co-administration of the CYP3A/1A2 inducer rifampicin reduced the average AUC of both single and multiple doses of anlotinib to 0.44-fold and 0.43-fold, respectively.

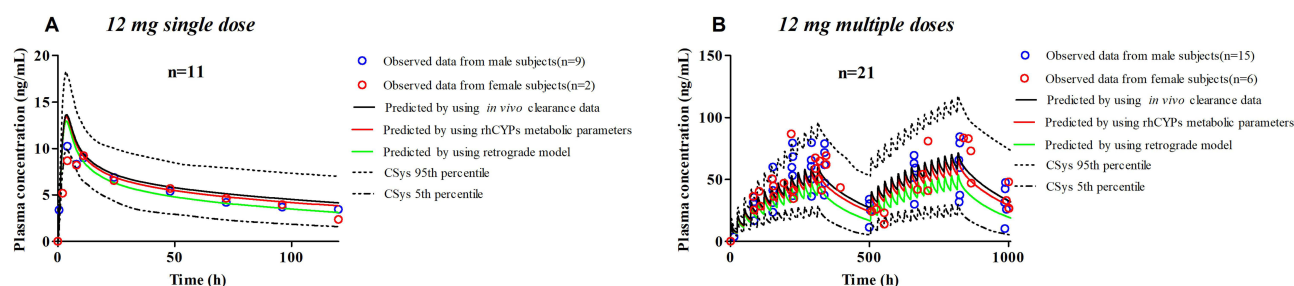


Figure 4 The validation of the anlotinib PBPK model was compared using three different methods, including *in vivo*, rhCYPs and retrograde techniques. **(A)** depicts predicted and observed plasma concentrations of anlotinib after a single dose of 12 mg. **(B)** represents predicted and observed plasma concentrations of anlotinib after multiple doses of 12 mg once daily for two courses.

In comparison to the default K_i values of perpetrators, simulations using experimentally determined K_i values still result in an $AUC_R < 1.5$ for co-administration, as demonstrated in [Figure S5](#) and [Table S4](#). The default K_i value of ketoconazole predicted a slightly higher DDI than the experimental K_i value, whereas for clarithromycin, the PK profile predicted from the default K_i value is almost identical to that predicted from the adjusted K_i . Furthermore, parameter sensitivity analysis indicates that the impact of K_i values on the AUC ratio of anlotinib is not significant, as depicted in [Figure 9](#). The maximum AUC ratio is expected to be 1.41 when K_i (CYP3A4) is 0.015 and K_i (CYP3A5) is 0.011.

Table 3 Pharmacokinetics of Single or Multiple Doses of Anlotinib with and without Coadministration of Perpetrators in Cancer Patients Predicted by Using rhCYP Method

	Group	Single Dose		Multiple Doses	
		C_{max} (ng/mL)	AUC_{last} (ng h/mL)	C_{max} (ng/mL)	AUC_{last} (ng h/mL)
No DDI	Anlotinib	13.43	1054.09	58.19	1252.77
Strong CYP3A inhibitor	With itraconazole	14.19	1262.86	67.76	1478.75
	Ratio	1.06	1.20	1.16	1.18
	With ketoconazole	14.47	1486.93	76.61	1710.48
	Ratio	1.08	1.41	1.32	1.37
	With clarithromycin	14.08	1415.48	71.34	1586.30
	Ratio	1.05	1.34	1.23	1.27
Moderate CYP3A inhibitor	With diltiazem	13.67	1176.76	62.54	1363.15
	Ratio	1.02	1.12	1.07	1.09
	With erythromycin	14.20	1461.11	73.59	1641.55
	Ratio	1.06	1.39	1.26	1.31
	With fluconazole	14.09	1364.28	70.72	1566.19
	Ratio	1.05	1.29	1.22	1.25
Strong CYP1A2 inhibitor	With fluvoxamine	13.89	1251.95	66.69	1461.94
	Ratio	1.03	1.19	1.15	1.17
	With ciprofloxacin	14.25	1317.74	70.13	1534.99
	Ratio	1.06	1.25	1.21	1.23
No DDI	Anlotinib	13.43	857.77	41.56	863.19
Strong CYP3A and moderate CYP1A2 inducer	With rifampicin	10.61	379.54	21.27	371.26
	Ratio	0.79	0.44	0.51	0.43

Notes: For the AUC ratio caused by inhibitors, a value greater than 2 indicates significant DDI; for the AUC ratio caused by inducers, a value less than 0.5 indicates significant DDI. The bold values indicate significant DDI.

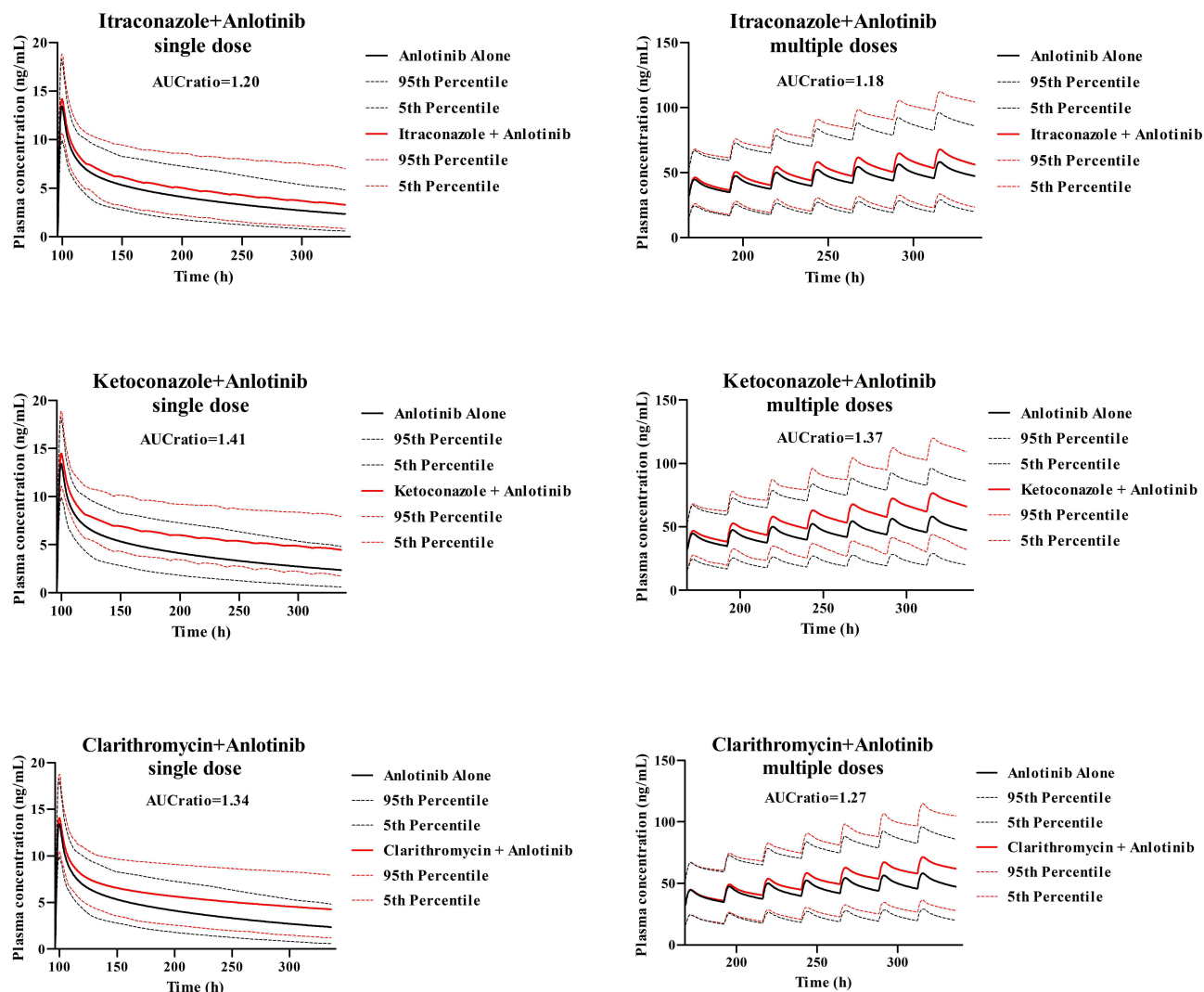


Figure 5 PBPK model-predicted plasma concentrations of anlotinib with (solid red lines) and without (solid black lines) co-administration of strong CYP3A inhibitors (itraconazole, ketoconazole, clarithromycin) in patients with cancer.

Discussion

At present, no formal clinical DDI studies have been conducted to investigate potential DDIs involving anlotinib and other drugs. Considering that cancer patients often require the administration of multiple medications, it is crucial to determine the potential risk of DDIs when combining anlotinib with other drugs. Thus, this study represents the first attempt to predict the DDI profile of anlotinib when it functions as a victim drug.

Anlotinib has been reported to be primarily metabolized by CYP3A4/5 and CYP1A2, which was confirmed in our *in vitro* metabolism experiments. We determined that the CL_{int} of anlotinib in human liver microsomal stability assay was $18 \mu\text{L}/\text{min}/\text{mg}$ protein, indicating a moderate metabolic rate in humans. Based on the CL_{int} classification bands for each species, a CL_{int} value of $\leq 8.6 \mu\text{L}/\text{min}/\text{mg}$ protein indicates a low metabolic rate, while a value $> 47 \mu\text{L}/\text{min}/\text{mg}$ protein indicates a high metabolic rate.¹⁸ Despite the drug label stating that anlotinib was metabolized by several enzymes, our results indicated that anlotinib was almost not metabolized by rCYP2B6, rCYP2C8, rCYP2C9, rCYP2D6, and rCYP2C19, as its depletion remained unchanged over different time points. Due to the lack of defined standards for metabolites, the enzyme kinetic parameters K_m and V_{max} for anlotinib cannot be obtained. Therefore, the current model only incorporates the CL_{int} parameters for anlotinib metabolized by different CYP enzymes. One shortcoming of such a model is that saturated metabolism cannot be modelled.

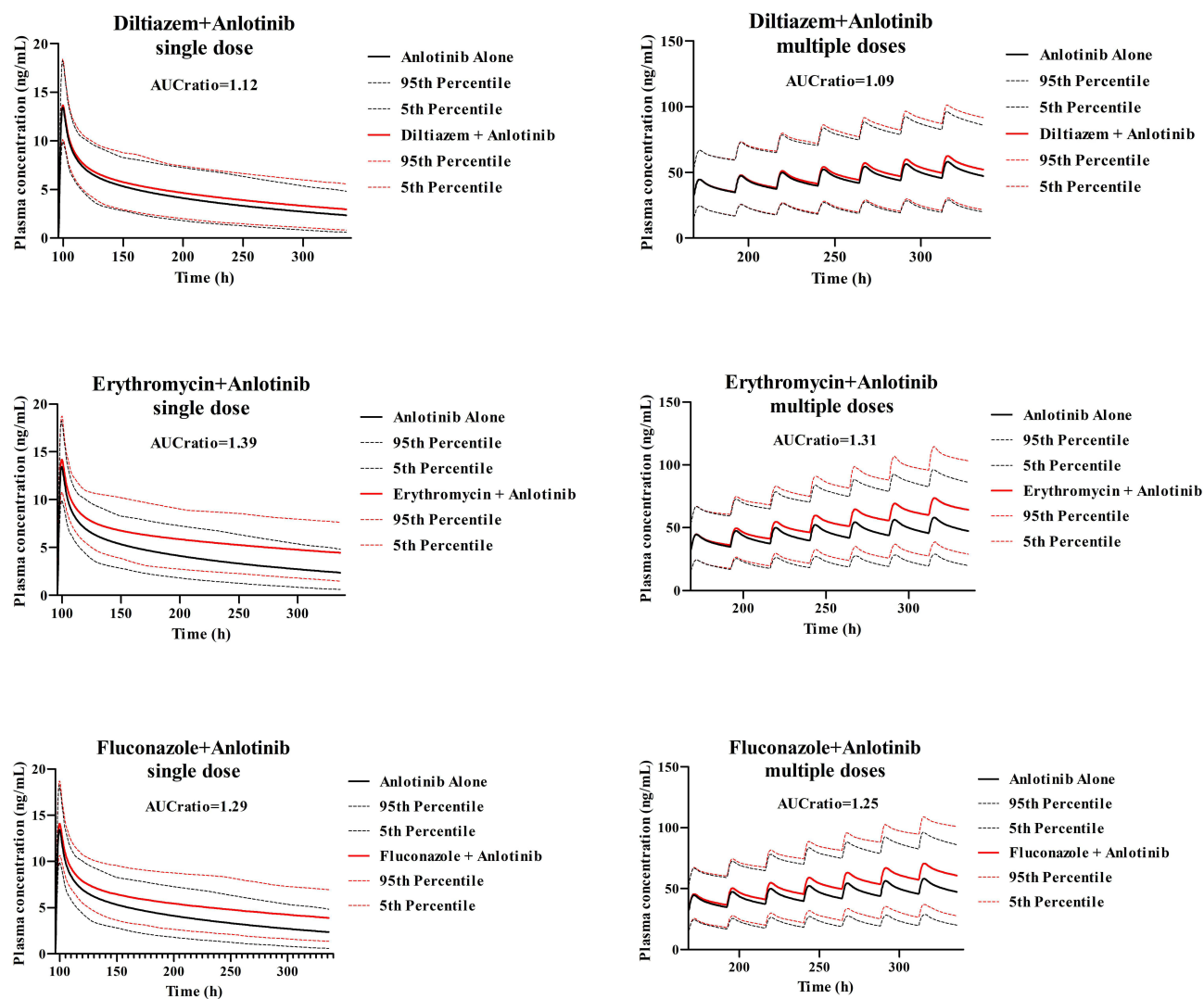


Figure 6 PBPK model-predicted plasma concentrations of anlotinib with (solid red lines) and without (solid black lines) coadministration of moderate CYP3A inhibitors (diltiazem, erythromycin, fluconazole) in patients with cancer.

To ensure the model better reflects the real conditions in the human body, the majority of the drug's ADME (Absorption, Distribution, Metabolism, and Excretion) parameters are sourced from humans, including apparent permeability through Caco-2 cells and intrinsic clearance values derived from human liver microsomes. In cases where human data are not available, we extrapolate data obtained from animal experiments to humans based on interspecies relationships, such as the tissue distribution of anlotinib in this study. In contrast to anlotinib as a perpetrator, the present PBPK model was developed using enzymatic kinetic parameters instead of *in vivo* clearance data. As a result, specific metabolic pathways involving enzymes were incorporated to refine the previously established anlotinib PBPK model. Additionally, the age of the virtual population has been changed from the default range of 20–50 years to 20–65 years, which better matches the age of cancer patients included in clinical trials using anlotinib.¹⁴ Through verification with different single and multiple doses, the PBPK model of anlotinib simulated using the rhCYP kinetic parameter exhibits better mechanistic performance compared to the *in vivo* parameter model, with accurate predictions within a 2-fold range for C_{\max} -ratio and AUC_{ratio} .⁶ To enhance the reliability of the PBPK model, a combination of ISEF-corrected rhCYPs kinetic parameters and retrograde model predicted from *in vivo* clearance data was employed. The distinction between rhCYPs and retrograde enzyme kinetic parameters lies in their respective modes of determination, with the former being directly measured experimentally and the latter being predicted.¹⁹ Generally, the retrograde model is employed to

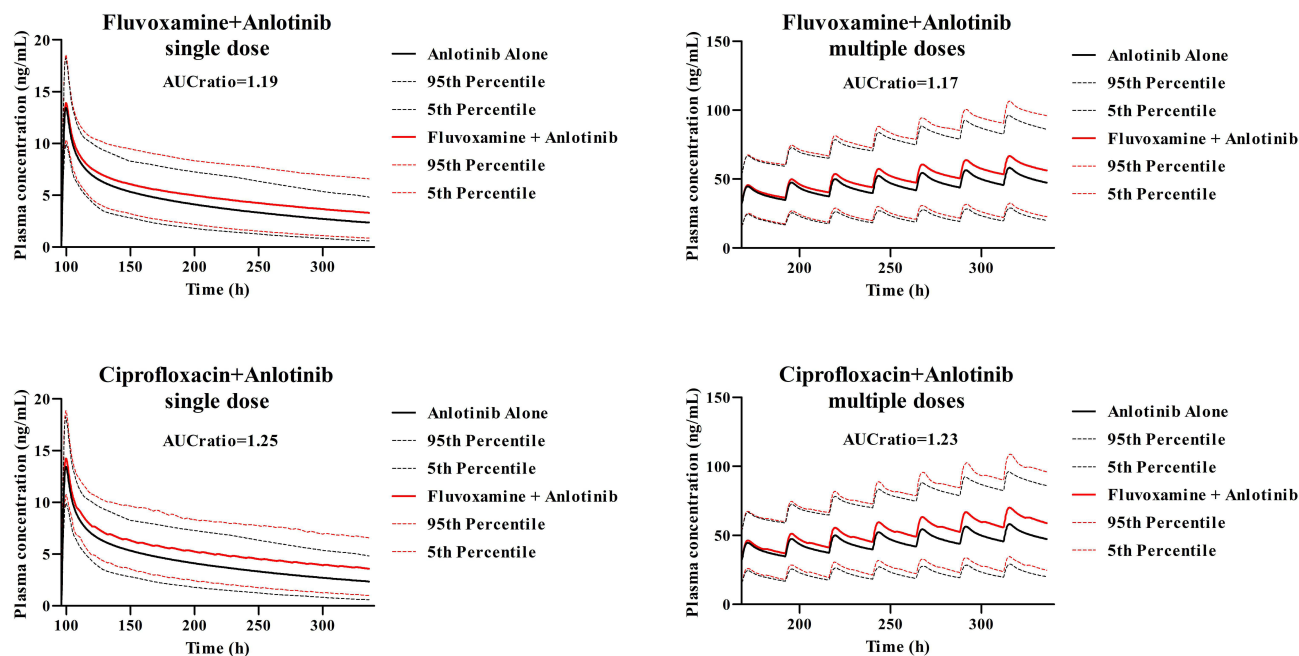


Figure 7 PBPK model-predicted plasma concentrations of anlotinib with (solid red lines) and without (solid black lines) coadministration of strong IA2 inhibitors (fluvoxamine, ciprofloxacin) in patients with cancer.

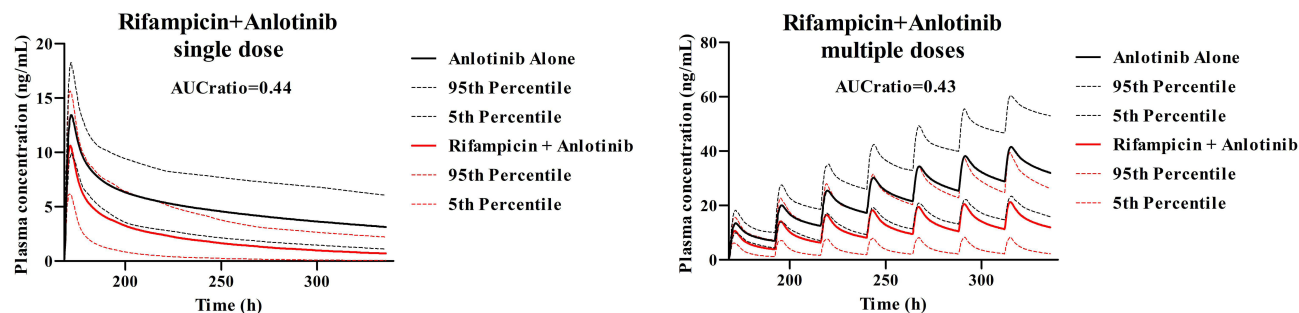


Figure 8 PBPK model-predicted plasma concentrations of anlotinib with (solid red lines) and without (solid black lines) coadministration of strong CYP3A and moderate CYP1A2 inducer (rifampicin) in patients with cancer.

forecast the intrinsic clearance of a given drug by specific CYP isoforms in the absence of experimental data. Here, we obtained the parameters of anlotinib metabolism by rhCYP through in vitro experiments. It was worth noting that, compared to the retrograde model, the pharmacokinetic characteristics of anlotinib predicted from rhCYPs experimental values better match the observed concentrations (as shown in [Figure S4](#) and [Table S3](#)). Therefore, in DDI prediction, we only chose the method of rhCYP parameter for prediction.

Regarding the design of DDI combination schemes, the simulation regimen was based on the clinical DDI studies of pyrotinib and itraconazole.²⁰ Moreover, a 4-day introduction period was designed to maximize the inhibition extent of inhibitors at steady state conditions. Given that anlotinib elimination was predicted to be slower after co-administration, the total simulation period was designed to be 336 hours. Furthermore, as complete induction was reported to be achieved one week after the initiation of rifampicin,²¹ a pre-induction period of seven days was also included.

The degree of increase in drug exposure resulting from reversible inhibition is associated with three key factors: the inhibitory potency (K_i), the concentration of the inhibitor, and the proportion of the drug that is typically metabolized by the inhibited enzyme.^{22,23} The K_i values obtained in the reversible inhibition studies were consistent with published values within an acceptable degree of accuracy. For instance, the K_i of ketoconazole was in the range of 0.05–11 μM ²⁴ and K_i of clarithromycin was in the range of 2.25–29.5 μM .²⁵ Analysis of the enzyme inhibition data suggested that the

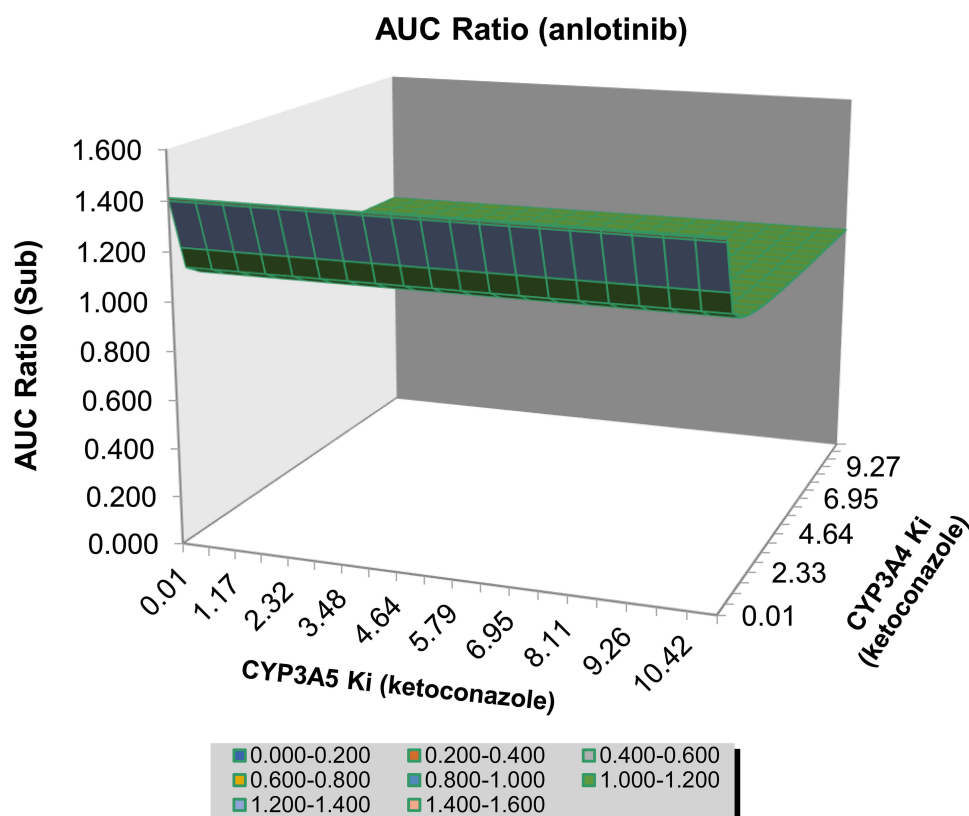


Figure 9 Parameter sensitivity analysis of K_i (CYP3A4 and CYP3A5) values of ketoconazole. Effect of changing ketoconazole K_i (CYP3A4 and CYP3A5) on predictions of the ketoconazole inhibition potential on anlotinib in cancer patients.

inhibition of anlotinib metabolism by ketoconazole, clarithromycin, and levofloxacin was best described by mixed inhibition. Compared to the default K_i values of perpetrators, simulations by entering experimentally measured K_i still show lower DDI exposure to anlotinib. Furthermore, the results of K_i sensitivity analysis demonstrated that the AUC ratio of anlotinib was not significantly influenced by K_i values. As a result, the default K_i values were adopted in the final DDI simulations. In addition, different inhibition mechanisms can also influence their drug interaction with anlotinib. Among all the inhibitors, clarithromycin, diltiazem and erythromycin exhibit both competitive inhibition and mechanism-based inhibition on CYP3A4.^{26,27} The fact that these inhibitors with mechanistic inhibition did not cause greater DDI is attributed to their low inactivation rate and low affinity. According to the classification by Ayah et al,²⁸ when K_{inact} is less than 0.05 s^{-1} (equivalent to $K_{inact} < 180 \text{ h}^{-1}$), it represents a low inactivation rate constant. If K_{app} is greater than 10 nM (equivalent to $K_{app} > 0.01 \text{ } \mu\text{M}$), it signifies low enzyme affinity. In the PBPK-DDI model, both inhibitory and induced effects of rifampicin are considered. As a consequence of prolonged administration, rifampicin exerts a prevailing induction effect. Moreover, despite being primarily recognized as a CYP3A inducer, rifampicin exhibits additional pharmacological characteristics by acting as a competitive inhibitor of the CYP3A4 enzyme.²⁹

According to the PBPK-DDI prediction results, enzyme inhibitors would unlikely result in a significant increase in single- or multi-dose anlotinib plasma exposure, with $\text{AUC}_{\text{ratio}}$ of 1.41 and 1.37 caused by ketoconazole, respectively. However, for DDI prediction with strong CYP3A inducers, our results showed a significant reduction in plasma exposure to a single dose of anlotinib after 14 days of co-administration with rifampicin, with an $\text{AUC}_{\text{ratio}}$ of 0.44. More importantly, this might lead to clinical failure of treatment. The DDI of multiple doses of anlotinib is basically the same. Although there is currently a lack of further clinical DDI studies to validate this prediction, our prior DDI prediction study employing anlotinib as a perpetrator indicated that anlotinib caused negligible alterations in both the AUC and C_{max} of S-warfarin, a representative CYP2C9 substrate. This finding is consistent with clinical reports, which did not observe any abnormal INR elevation or bleeding when anlotinib was co-administered with warfarin.³⁰ This also reflects the reliability of the model predictions when anlotinib

is used as a victim drug. Similarly, in clinical practice, we can observe whether there is an increase in adverse drug reactions such as bleeding or elevated blood pressure when anlotinib is co-administered with CYP inhibitors.³¹ In addition, the situation in which anlotinib is affected by CYP enzyme modulators is similar to other TKIs metabolized through CYP3A4. Co-administration of erlotinib with CYP3A4 inhibitors, such as ketoconazole and ritonavir, led to a significant alteration in erlotinib exposure, as evidenced by a 1.7- and 3.0-fold increase in erlotinib AUC, respectively.³² Similarly, the $AUC_{0-\infty}$ and C_{max} of zanubrutinib were increased by 3.8-fold and 2.6-fold, respectively, following co-administration with itraconazole, but no significant increase in adverse effect was observed.²⁰ It was found that rifampicin reduced the $AUC_{0-\infty}$ and C_{max} of erlotinib to 0.33-fold and 0.71-fold, respectively, in cancer subjects.³³ Carbamazepine, a potent CYP3A4 inducer, was found to significantly reduce the geometric mean of lapatinib AUC and C_{max} by 72% and 59%, respectively.³⁴

Metabolic enzyme gene polymorphisms were not considered in this study, as well as the PK-PD relationship of anlotinib. Currently, there are few studies on genetic polymorphisms in the metabolizing enzymes of anlotinib. Tan et al conducted a single-center retrospective study to investigate the relationship between CYP450 gene polymorphisms, anlotinib concentrations, and their adverse reactions in Chinese patients with lung cancer. Their findings suggested that the clinical correlation of anlotinib plasma exposure resides not in mutations of CYP3A4 and CYP3A5, but rather in mutations of CYP2C19.³⁵ However, the authors did not provide an explanation for the occurrence of this phenomenon, and the entire text also does not mention the metabolism of anlotinib via CYP2C19.

In general, due to the high cost of anlotinib, with an approximate price of 514 CNY per tablet (equivalent to approximately 71 USD), it is recommended to avoid concomitant use with strong CYP inducers like rifampicin. Instead, a drug with a relatively weak induction and similar anti-infective effect may be considered.

Limitations

Our research also has its limitations. First, the results suggest that CYP3A4 inductions may significantly lower anlotinib systemic exposure. However, this needs to be verified through clinical testing. In addition, there is a lack of dose-response relationship studies in the field of pharmacokinetics-pharmacodynamics (PK-PD) for anlotinib. In the future, there is a great potential for research on the PK-PD of antitumor drugs, as well as further development and application of model prediction. This will contribute to optimizing drug treatment strategies, individualized medication, and improving therapeutic outcomes.

Conclusion

In summary, we constructed and validated a PBPK model for anlotinib as a victim drug and predicted its pharmacokinetic interactions with typical CYP3A/1A2 inhibitors and inducers. Our predictions suggest that: 1) Co-administration of anlotinib with CYP3A/1A2 inhibitors, including ketoconazole, itraconazole, clarithromycin, diltiazem, erythromycin, fluconazole, fluvoxamine, and ciprofloxacin, does not cause significant anlotinib interactions. However, it is crucial to closely monitor for anlotinib-related adverse reactions, such as bleeding and hypertension. 2) It is noteworthy that long-term concurrent use of anlotinib with potent CYP enzyme inducers should be avoided. What's more, further clinical DDI disclosures can validate our predictions.

Data Sharing Statement

The authors declare that all the data supporting the findings of this study are available within the paper and its Supplemental Materials.

Acknowledgments

An academic license has been granted by Certara UK (Simcyp Division) to give free access to Simcyp[®] Simulators.

Funding

This study was supported by the National Natural Science Foundation of China and the National Research Foundation of Korea (No. 82011540409) and under the framework of an international cooperation program managed by the National Research Foundation of Korea (2020K2A9A2A06064919).

Disclosure

The authors declared no potential conflicts of interest in this work.

References

1. Chen P, Liu Y, Wen Y, et al. Non-small cell lung cancer in China. *Cancer Commun.* 2022;42(10):937–970. doi:10.1002/cac2.12359
2. Siegel RL, Miller KD, Fuchs HE, et al. Cancer statistics, 2022. *CA Cancer J Clin.* 2022;72(1):7–33. doi:10.3322/caac.21708
3. Sculier JP, Paesmans M, Libert P, et al. Long-term survival after chemotherapy containing platinum derivatives in patients with advanced unresectable non-small cell lung cancer. *European Lung Cancer Working Party. Eur J Cancer.* 1994;30A(9):1342–1347. doi:10.1016/0959-8049(94)90184-8
4. Zhong CC, Chen F, Yang JL, et al. Pharmacokinetics and disposition of anlotinib, an oral tyrosine kinase inhibitor, in experimental animal species. *Acta Pharmacol Sin.* 2018;39(6):1048–1063. doi:10.1038/aps.2017.199
5. National Medical Products Administration. Drug label of anlotinib. Available from: <https://zy.yaozh.com/instruct/sms20210430/2021033006.pdf>. Accessed Feb 22, 2022.
6. Jin Z, He Q, Zhu X, et al. Application of physiologically based pharmacokinetic modelling for the prediction of drug-drug interactions involving anlotinib as a perpetrator of cytochrome P450 enzymes. *Basic Clin Pharmacol Toxicol.* 2022;130(5):592–605. doi:10.1111/bcpt.13721
7. Shebley M, Sandhu P, Emami Riedmaier A, et al. Physiologically based pharmacokinetic model qualification and reporting procedures for regulatory submissions: a consortium perspective. *Clin Pharmacol Ther.* 2018;104(1):88–110. doi:10.1002/cpt.1013
8. Grimstein M, Yang Y, Zhang X, et al. Physiologically based pharmacokinetic modeling in regulatory science: an update from the U.S. food and drug administration's office of clinical pharmacology. *J Pharm Sci.* 2019;108(1):21–25. doi:10.1016/j.xphs.2018.10.033
9. U.S. Food and Drug Administration. Clinical drug interaction studies-cytochrome P450 Enzyme- and transporter-mediated drug interactions guidance for industry; 2020. Available from: <https://www.fda.gov/media/134581/download>. Accessed October 09, 2024.
10. Obach RS. Prediction of human clearance of twenty-nine drugs from hepatic microsomal intrinsic clearance data: an examination of in vitro half-life approach and nonspecific binding to microsomes. *Drug Metab Dispos.* 1999;27(11):1350–1359.
11. Attwa MW, Abdelhameed AS, Kadi AA. LC-MS/MS estimation of rociletinib levels in human liver microsomes: application to metabolic stability estimation. *Drug Des Devel Ther.* 2021;15:3915–3925. doi:10.2147/DDDT.S321330
12. Umehara KI, Huth F, Gu H, et al. Estimation of fractions metabolized by hepatic CYP enzymes using a concept of inter-system extrapolation factors (ISEFs) - A comparison with the chemical inhibition method. *Drug Metab Pers Ther.* 2017;32(4):191–200. doi:10.1515/dmpt-2017-0024
13. Schulz J, Thomas A, Saleh A, et al. Towards the elucidation of the pharmacokinetics of voriconazole: a quantitative characterization of its metabolism. *Pharmaceutics.* 2022;14(3):477. doi:10.3390/pharmaceutics14030477
14. Sun Y, Niu W, Du F, et al. Safety, pharmacokinetics, and antitumor properties of anlotinib, an oral multi-target tyrosine kinase inhibitor, in patients with advanced refractory solid tumors. *J Hematol Oncol.* 2016;9(1):105. doi:10.1186/s13045-016-0332-8
15. Zhang H, Bu F, Li L, et al. Prediction of drug-drug interaction between tacrolimus and principal ingredients of wuzhi capsule in Chinese healthy volunteers using physiologically-based pharmacokinetic modelling. *Basic Clin Pharmacol Toxicol.* 2018;122(3):331–340. doi:10.1111/bcpt.12914
16. Wagner C, Pan Y, Hsu V, et al. Predicting the effect of cytochrome P450 inhibitors on substrate drugs: analysis of physiologically based pharmacokinetic modeling submissions to the US Food and Drug Administration. *Clin Pharmacokinet.* 2015;54(1):117–127. doi:10.1007/s40262-014-0188-4
17. Wagner C, Pan Y, Hsu V, et al. Predicting the Effect of CYP3A Inducers on the Pharmacokinetics of Substrate Drugs Using Physiologically Based Pharmacokinetic (PBPK) Modeling: an Analysis of PBPK Submissions to the US FDA. *Clin Pharmacokinet.* 2016;55(4):475–483. doi:10.1007/s40262-015-0330-y
18. Houston JB. Utility of in vitro drug metabolism data in predicting in vivo metabolic clearance. *Biochem Pharmacol.* 1994;47(9):1469–1479. doi:10.1016/0006-2952(94)90520-7
19. Michelet R, Van Bocxlaer J, Allegaert K, et al. The use of PBPK modeling across the pediatric age range using propofol as a case. *J Pharmacokinet Pharmacodyn.* 2018;45(6):765–785. doi:10.1007/s10928-018-9607-8
20. Liu Y, Zhang Q, Lu C, et al. Multiple administrations of itraconazole increase plasma exposure to pyrotinib in Chinese healthy adults. *Drug Des Devel Ther.* 2021;15:2485–2493. doi:10.2147/DDDT.S312310
21. Cai MM, Dou T, Tang L, et al. Effects of rifampicin on antineoplastic drug pyrotinib maleate pharmacokinetics in healthy subjects. *Invest New Drugs.* 2022;40(4):756–761. doi:10.1007/s10637-022-01241-7
22. Yao C, Levy RH. Inhibition-based metabolic drug-drug interactions: predictions from in vitro data. *J Pharmaceut Sci.* 2002;91(9):1923–1935. doi:10.1002/jps.10179
23. Ito K, Brown HS, Houston JB. Database analyses for the prediction of in vivo drug-drug interactions from in vitro data. *J Pharm Sci.* 2004;57(4):473–486. doi:10.1002/jps.10179
24. Greenblatt DJ, Venkatakrishnan K, Harmatz JS, et al. Sources of variability in ketoconazole inhibition of human cytochrome P450 3A in vitro. *Xenobiotica.* 2010;40(10):713–720. doi:10.3109/00498254.2010.506224
25. Polasek TM, Miners JO. Quantitative prediction of macrolide drug-drug interaction potential from in vitro studies using testosterone as the human cytochrome P4503A substrate. *Eur J Clin Pharmacol.* 2006;62(3):203–208. doi:10.1007/s00228-005-0091-x
26. Zhou S, Yung Chan S, Cher Goh B, et al. Mechanism-based inhibition of cytochrome P450 3A4 by therapeutic drugs. *Clin Pharmacokinet.* 2005;44(3):279–304. doi:10.2165/00003088-200544030-00005
27. Quinney SK, Zhang X, Luksiri A, et al. Physiologically based pharmacokinetic model of mechanism-based inhibition of CYP3A by clarithromycin. *Drug Metab Dispos.* 2010;38(2):241–248. doi:10.1124/dmd.109.028746
28. Abdeldayem A, Raouf YS, Constantinescu SN, et al. Advances in covalent kinase inhibitors. *Chem Soc Rev.* 2020;49(9):2617–2687. doi:10.1039/c9cs00720b
29. Chattopadhyay N, Kanacher T, Casjens M, et al. CYP3A4-mediated effects of rifampicin on the pharmacokinetics of vilaprisan and its UGT1A1-mediated effects on bilirubin glucuronidation in humans. *Br J Clin Pharmacol.* 2018;84(12):2857–2866. doi:10.1111/bcp.13750

30. Fu Y, Huang J, Wu L, Gao Q. Rationality evaluation of using small-molecular targeted drugs in patients with non-small cell lung cancer in a hospital. *China Pharmaceut.* 2023;32(3):110–115. In Chinese.
31. Li S, Wang H. Research progress on mechanism and management of adverse drug reactions of anlotinib. *Drug Des Devel Ther.* 2023;17:3429–3437. doi:10.2147/DDDT.S426898
32. Deeken JF, Beumer JH, Anders NM, et al. Preclinical assessment of the interactions between the antiretroviral drugs, ritonavir and efavirenz, and the tyrosine kinase inhibitor erlotinib. *Cancer Chemother Pharmacol.* 2015;76(4):813–819. doi:10.1007/s00280-015-2856-y
33. Hamilton M, Wolf JL, Drolet DW, et al. The effect of rifampicin, a prototypical CYP3A4 inducer, on erlotinib pharmacokinetics in healthy subjects. *Cancer Chemother Pharmacol.* 2014;73(3):613–621. doi:10.1007/s00280-014-2390-3
34. Smith DA, Koch KM, Arya N, et al. Effects of ketoconazole and carbamazepine on lapatinib pharmacokinetics in healthy subjects. *Br J Clin Pharmacol.* 2009;67(4):421–426. doi:10.1111/j.1365-2125.2009.03370.x
35. Tan T, Han G, Cheng Z, et al. Genetic polymorphisms in CYP2C19 cause changes in plasma levels and adverse reactions to anlotinib in Chinese patients with lung cancer. *Front Pharmacol.* 2022;13:918219. doi:10.3389/fphar.2022.918219

Drug Design, Development and Therapy

Dovepress

Publish your work in this journal

Drug Design, Development and Therapy is an international, peer-reviewed open-access journal that spans the spectrum of drug design and development through to clinical applications. Clinical outcomes, patient safety, and programs for the development and effective, safe, and sustained use of medicines are a feature of the journal, which has also been accepted for indexing on PubMed Central. The manuscript management system is completely online and includes a very quick and fair peer-review system, which is all easy to use. Visit <http://www.dovepress.com/testimonials.php> to read real quotes from published authors.

Submit your manuscript here: <https://www.dovepress.com/drug-design-development-and-therapy-journal>